



Cite this: DOI: 10.1039/c4dt03578j

A blue luminescent MOF as a rapid turn-off/ turn-on detector for H₂O, O₂ and CH₂Cl₂, MeCN: $\overset{3}{\infty}[\text{Ce}(\text{Im})_3\text{ImH}]\cdot\text{ImH}\dagger$

L. V. Meyer,^a F. Schönfeld,^a A. Zurawski,^a M. Mai,^b C. Feldmann^b and
K. Müller-Buschbaum^{*a}

The blue emitting luminescent MOF $\overset{3}{\infty}[\text{Ce}(\text{Im})_3\text{ImH}]\cdot\text{ImH}$ forms a 3D-framework with Kagomé net topology. The framework exhibits an intense blue luminescence which can be retained upon activation of the MOF with the formula $\overset{3}{\infty}[\text{Ce}(\text{Im})_3\text{ImH}]$. The luminescence is metal-based due to parity-allowed 5d–4f-transitions. Time-dependent investigations of the interaction with liquid and gas analytes show that the MOF – by utilising 5d–4f-transitions of Ce³⁺ – can be used as a high-speed “turn-off” detector for water and oxygen in dry air. Other protic or polar solvents, like methanol, acetone or pyridine, which also show a “turn-off”-effect can be distinguished from water-detection either on a time scale (ranging up to 250 000 : 1) or a shift of the chromaticity, the latter being pronounced for MeOH. The fast time-dependent decrease of the luminescence intensity for water arises from an extremely fast hydrolysis and is irreversible. Polar aprotic molecules like dichloromethane and acetonitrile can also result in a “turn-on”-effect of the luminescence intensity due to their behaviour as additional sensitizers for Ce³⁺-emission. We conclude that the cerium-MOF can be utilised in gas and liquid sensing applications as a detector material for water and oxygen in dry air. The luminescence is intense with good quantum yield between 55% (as-synthesised) and 36% (activated). This implies that only milligram amounts of the material are needed to detect the analyte species and is especially useful, as the MOF can be directly used as-synthesised for water detection in applications for which an irreversible signal change is desired, e.g. preventing a signal change upon unwanted re-drying.

Received 21st November 2014,

Accepted 14th January 2015

DOI: 10.1039/c4dt03578j

www.rsc.org/dalton

Introduction

Metal organic frameworks (MOFs) have made a significant impact on the field of materials science since their initial discovery.^{1–3} Renowned for their microporosity,⁴ MOFs also display a variety of important properties as their secondary characteristics, such as magnetism,⁵ catalytic activity⁶ and photoluminescence.^{7–9} This is leading to a growing field of study of materials with various potential applications that can be modified by variations of linkers, metals, templating mole-

cules and synthetic approaches. A major focus in recent years has been the development of MOFs for sensing applications by using changes in photoluminescence properties caused by host–guest interactions as interpretable signals.¹⁰ For such applications, two different sensing principles have been reported. The first of these relies upon a distinct and large change in the luminescence intensity upon interaction with the analyte species, leading to a turn-off or turn-on effect for the luminescence as an observable/measurable parameter.¹¹ For example an efficient quenching of the luminescence can be used for sensing if the effect is selective to a certain molecule, ion, *etc.* Such effects have been recently shown for the sensing of O₂-gas using the porosity of MOF UiO-67 (Zr₆O₄(OH)₄(bpdc)₆, bpdc^{2–} = *para*-biphenyldicarboxylate) for loading with phosphorescent Ir³⁺-complexes. Interaction of these complexes with O₂ leads to quenching, whereas no sensitivity is observed for N₂.¹² Different intensity changes can also be utilised to track different analyte species, as shown for the turn-off sensing of different nitro-aromatics by fluorescent Zn-based MOFs like [Zn₂(bpdc)₂bpee] (bpdc^{2–} = 4,40-biphenyldicarboxylate; bpee = 1,2-bipyridylethene), meaning they are

^aInstitute of Inorganic Chemistry, Julius-Maximilians-University Würzburg, Am Hubland, 97074 Würzburg, Germany.

E-mail: k.mueller-buschbaum@uni-wuerzburg.de; Fax: +49-931-3184785;

Tel: +49-931-3188724

^bInstitute of Inorganic Chemistry, Karlsruhe Institute of Technology (KIT), Engesserstr. 15, 76131 Karlsruhe, Germany

† Electronic supplementary information (ESI) available: DTA/TG investigations, experimental details, crystallographic and powder diffraction data, photoluminescence spectra showing turn-off and turn-on effects. CCDC 1027917. For ESI and crystallographic data in CIF or other electronic format see DOI: 10.1039/c4dt03578j

capable of detecting explosives.¹³ Recently, the europium MOF [Eu₃(MFDA)₄(NO₃)(DMF)₃] (H₂MFDA = 9,9-dimethylfluorene-2,7-dicarboxylic acid) was shown to have variable quenching for ten different nitro aromatic systems, with the highest quenching observed for 3,4-dinitrotoluene (3,4-DNT) and 1,2-dinitrobenzene (1,2-DNB).¹⁴ The contrasting process, a turn-on of luminescence, is also of interest and can arise from an analyte that acts as a sensitizer for a luminescence process that would not be otherwise observable. An example of this was shown for [Eu(BTPCA)(H₂O)], BTPCA³⁻ = 1,1',1''-(benzene-1,3,5-triyl)tripiperidine-4-carboxylate, in which binding to Zn²⁺ leads to a remarkable increase of the Eu³⁺ emission intensity.¹⁵

The second possibility for luminescence sensing by a MOF is by a change of the luminescence colour upon interaction of the MOF with the analyte.^{10,11} This occurs as a result of the analyte influencing relevant energy levels involved in the luminescence process without quenching the luminescence. Such a process was successfully shown for different simple aromatic ligands interacting with the MOF. A representative example is the use of zinc containing IRMOFs to detect benzene and some of its derivatives like Tol, MePh, PhCN or PhOMe. Interaction of the IRMOF leads to a bathochromic shift of the MOF fluorescence over the complete visible spectrum from benzonitrile to iodobenzene.¹⁶ In addition to the detection of gas and liquid molecules, the sensing of metal ions besides Zn²⁺ has also been shown for other transition metal ions and lanthanides.¹⁷ It is evident that for sensing applications the sensor must be fast, sensitive and at best selective for only a few different analytes. This limits the current number of known suitable luminescence sensors to a small number of MOFs. Thus the identification of new MOFs as potential sensors is an attractive idea.

In recent years, imidazolate MOFs have been highlighted for use as ZIFs due to their capability of adopting zeolite structures if the metal centre is four-coordinate. In addition, metal ions with large coordination numbers (CN) can lead to interesting MOFs, *e.g.* when combined with lanthanide ions as they offer multifunctionality constituted by functions like porosity and luminescent properties. However, the high CN limits the inner surface of the materials. We have previously shown that reacting lanthanide metals with melts of heterocyclic amines like azoles leads to a variety of photoluminescent frameworks,^{18–22} some of the most potent and efficient emitters being imidazolates. Herein, we wish to elaborate on the formation of a previously unknown cerium-based imidazolate framework, ³[Ce(Im)₃ImH], that shares structural characteristics with the framework ³[Pr(Im)₃(ImH)].²³ The compound ³[Ce(Im)₃ImH]-ImH (**1**) is obtained by reacting elemental cerium with a self-consuming melt of the linker molecule 1*H*-imidazole and exhibits an intense blue photoluminescence originating from f–d-transitions. Further studies show microporosity upon activation as well as capable function as an analyte specific detector. This can be related to rapid changes in the photoluminescence intensity upon exposure to various analyte gases and liquids.

Results and discussion

Crystal structure, topology, thermal properties, porosity and adsorption

The compound ³[Ce(Im)₃ImH]-ImH (**1**) crystallizes in the monoclinic crystal system with the space group *P2₁/n*, and is isotopic to ³[Pr(Im)₃ImH]-ImH.²³ The four crystallographically independent Ce-atoms each are surrounded by seven N-atoms. The coordination sphere of three of the Ce-atoms can be described as a single-capped trigonal prism. The coordination sphere of the fourth Ce-site can be described as a pentagonal bipyramid. In all polyhedra, six edges are occupied by μ-1κ¹:2κ³-bridging imidazolate anions (Im⁻), while one edge is occupied by a neutral end-on coordinating imidazole molecule (ImH), resulting in trivalent Ce-atoms (Fig. 1, bottom). Six imidazolate anions connect four cations resulting in a P₄O₆-analogous pseudo-tetrahedral Ce₄(Im)₆-unit (Fig. 1, top). Connecting them further *via* sides and corners yields a three dimensional network (Fig. 2, left). The resulting topology can be described as four two-dimensional Kagome-like 3,4-networks (Fig. 2, right). Based on this 3,4-net parallel to the (110)-plane, three additional distorted Kagomé nets share common vertices with the initial base net. These three nets are arranged in 126°, 115° and 112°, respectively, with respect to their common base net. The framework exhibits an extensive channel system along all three cell axes.

To indicate phase purity and high yields of **1**, the results of PXRD investigations were compared to single crystal data and are shown in Fig. 3. Due to the higher Coulomb participation, the amide bonds between imidazolate anions and Ce-atoms are about 8–14 pm shorter than the amine bonds of the end-on imidazole ligands.

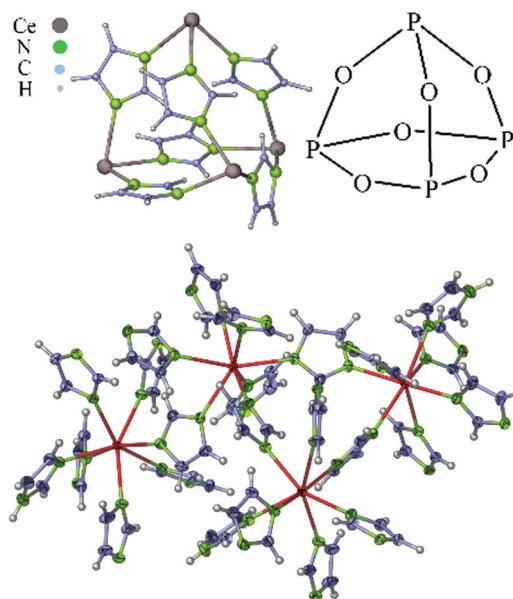


Fig. 1 Coordination sphere of the Ce atoms in ³[Ce(Im)₃ImH]-ImH (bottom) with a probability level of the atoms of 50% and a Ce₄(Im)₆-unit in comparison with P₄O₆ (top).

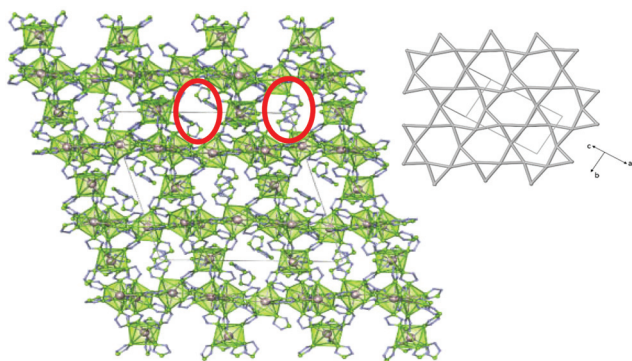


Fig. 2 Crystal structure of ${}^3[\text{Ce}(\text{Im})_3\text{ImH}] \cdot \text{ImH}$ (**1**) view along [010] (left), with ImH occupied channels (red circles); one of the two-dimensional kagome-like 3,4-networks (right).

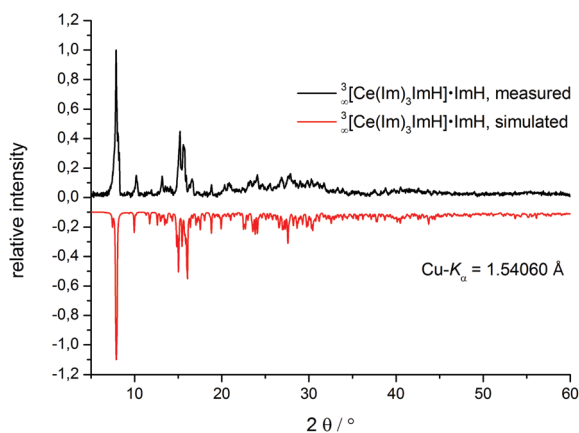


Fig. 3 Powder diffractogram of bulk **1** (black) compared to powder diffractogram of simulated single crystal data of **1** (red).

In accordance with the lanthanide contraction, the Ce–N distances are longer than the Pr–N distances in the isotopic compound ${}^3[\text{Pr}(\text{Im})_3(\text{ImH})] \cdot \text{ImH}$.²³ The angles N–Ln–N are in the same range in both compounds. The Ce–N distances are in the range of 2521(3)–2657(3) pm and accord well with the former published ${}^1[\text{Ce}(\text{Btz})_3(\text{BtzH})] \cdot \text{ImH}$ as well as $[\text{Ce}(\text{triRNTB})_2] \cdot (\text{CF}_3\text{SO}_3)_3$ (triRNTB = tris(*N*-alkylbenzimidazol-2-ylmethyl)amine).²⁵ The pores of **1** provide a maximum diameter of 760 pm with apertures of 580 pm when taking hydrogen van-der-Waals radii²⁶ into consideration.

Simultaneous DTA/TG investigations on ${}^3[\text{Ce}(\text{Im})_3(\text{ImH})] \cdot \text{ImH}$ (**1**) exhibit two endothermic signals at 175 and 245 °C with a subsequent mass loss of 26% (see Fig. S1, ESI†). Given that one equivalent of imidazole corresponds to 14% of the overall mass, the mass loss of 26% can be attributed to the loss of the two imidazole molecules: an initial loss of the intercalated imidazole equivalent having the formula ${}^3[\text{Ce}(\text{Im})_3(\text{ImH})]$ and subsequently, to the loss of the coordinating imidazole molecule and $[\text{Ce}(\text{Im})_3]$. The initial release step gives a value for the imidazole release of about 3% less than the expected value. This can be explained by an observed partial loss of imidazole during the workup processes (sublimation of

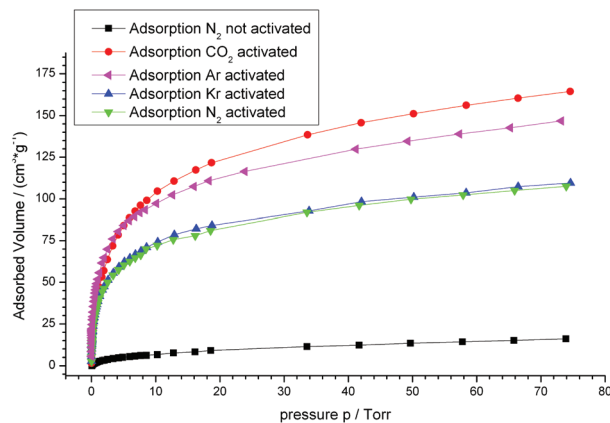


Fig. 4 Adsorption isotherms according to BET on activated **1**, indicating microporosity together with a preference for CO_2 adsorption.

excess imidazole). These findings corroborate the results of the elemental analysis, which also show a slight reduction (calcd C, 37.73; N, 29.33; H, 3.59. Found C, 36.62; N, 28.24; H, 3.42%). It is most likely that non-coordinating imidazole molecules are released initially, before coordinating *end-on* imidazole molecules are released. The resulting compound with the constitution $[\text{Ce}(\text{Im})_3]$ is thermally stable up to 550 °C.

In order to prove the MOF character and potential microporosity, **1** was activated at 225 °C at 10^{-3} mbar for 4.5 h. Adsorption–desorption isotherms were recorded by BET investigations for N_2 , Ar, CO_2 , and Kr (–196 °C for N_2 , and Ar, as well as –75 °C for CO_2 , and –153 °C for Kr) in the relative pressure range 10^{-6} to 1 atm. The results were compared to the non-activated framework. While the non-activated framework is dense simply due to the occupied pores, significant amounts of all gases investigated can be incorporated into the activated MOF (see Fig. 4). In addition, the MOF shows the highest preference for CO_2 adsorption giving an uptake of $160 \text{ cm}^3 \text{ g}^{-1}$ followed by Ar adsorption ($135 \text{ cm}^3 \text{ g}^{-1}$), whereas only $85 \text{ cm}^3 \text{ g}^{-1}$ of N_2 and Kr could be adsorbed. This corresponds to a moderate surface area of $S_{\text{BET}} = 480 \text{ m}^2 \text{ g}^{-1}$ for CO_2 adsorption at –75 °C. We also tried high-pressure CO_2 adsorption up to 45 bar at 50 °C, but decomposition stops the adsorption process for this CO_2 pressure. The lower uptake Kr and N_2 can be explained by the atom size and the kinetic diameter, respectively. The observed preference for CO_2 may be a result of the oxophilicity of the lanthanide cerium in **1**.

Photoluminescence properties and sensing studies for liquids and gases

Both the as-synthesised and the activated compound **1** show an intense blue luminescence under UV-excitation (Fig. 5) that does not change upon activation. The identical shapes of the photoluminescence spectra prove that the chemical surrounding of cerium is maintained upon activation and that no structural collapse occurs. This is very useful, especially, as PXRD is not possible.

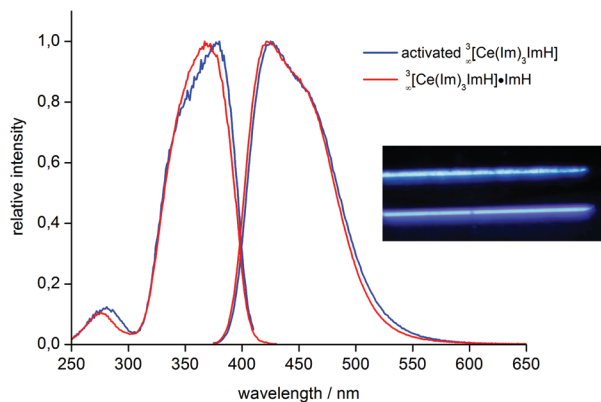


Fig. 5 Normalised excitation and emission spectra of as-synthesised and activated **1** (left); visible blue emission of as-synthesised (bottom) and activated **1** (top) under UV excitation ($\lambda_{\text{Exc}} = 366 \text{ nm}$) (right).

The luminescence of Ce^{3+} is based on parity allowed 4f–5d transitions for excitation and *vice versa* 5d–4f transitions for emission. Typically, 5d–4f transitions of lanthanide ions mainly occur in the UV region due to 5d states lying at high energy for most lanthanide ions. Besides Eu^{2+} , Ce^{3+} is an exception among the trivalent lanthanide ions as it can provide 5d–4f transitions $<33\,000 \text{ cm}^{-1}$ by crystal and ligand-field splitting.²⁷ Depending on the chemical surrounding of the Ce^{3+} ions, these transitions can be shifted to lower energies. This is a prominent feature of the $\text{Y}_3\text{Al}_5\text{O}_{12}:\text{Ce}^{3+}$ laser (YAG:Ce) that emits in the yellow region.²⁸ Due to the participation of d-states, and thus due to the strong influence of both ligands and crystal fields, excitation and emission energies are dependent on the chemical surrounding. This results in a blue luminescence for as-synthesised ${}^3[\text{Ce}(\text{Im})_3\text{ImH}] \cdot \text{ImH}$ and activated ${}^3[\text{Ce}(\text{Im})_3\text{ImH}]$. The parity allowed character of these transitions is responsible for a high transition probability and thus intense luminescence of **1**. The excitation of Ce^{3+} occurs *via* promotion of the 4f¹ ground state into the 4f⁰5d¹-level. Due to the nephelauxetic effect, 5d-levels are lowered in energy and split (crystal field splitting) in the coordinated sphere compared to free Ce^{3+} . The broad emission occurs upon relaxation from 4f⁰5d¹-levels into 4f¹-levels (${}^2\text{F}_{5/2}$ and ${}^2\text{F}_{7/2}$) that are split by spin orbit coupling.

The excitation spectra of **1** exhibit a maximum at $\lambda = 367 \text{ nm}$ and a weaker second maximum at $\lambda = 276 \text{ nm}$. The weaker additional maximum can be addressed to an excited *S-state of the ligand.^{19,29} The emission maximum is located at $\lambda = 422 \text{ nm}$. The absolute quantum yield was determined to be $\text{QY} = 55\%$ ($\lambda_{\text{Exc}} = 366 \text{ nm}$) and shows that a high amount of absorbed light is reemitted. For the activated MOF, the first and second excitation maxima are at $\lambda = 380 \text{ nm}$ and $\lambda = 281 \text{ nm}$, the emission maximum is $\lambda = 425 \text{ nm}$. In comparison with the as-synthesised MOF, the absolute quantum yield decreases to $\text{QY} = 36\%$ ($\lambda_{\text{Exc}} = 366 \text{ nm}$), indicating a sensitizer effect of the intercalated imidazole in the as-synthesised MOF. In Table 2 the significant luminescence data for as-synthesised and activated **1** are reported. Both the non-activated and the

Table 1 Crystallographic data of ${}^3[\text{Ce}(\text{Im})_3\text{ImH}] \cdot \text{ImH}$ (**1**). Standard deviations are given in brackets

Empirical formula	$\text{C}_{15}\text{H}_{17}\text{N}_{10}\text{Ce}$
M_r	477.51
Crystal system	Monoclinic
Space group	$P2_1/n$
a/pm	2325.3(5)
b/pm	1402.4(3)
c/pm	2345.5(5)
$\beta/^\circ$	107.7(1)
$V/10^6 \cdot \text{pm}^3$	7288(3)
Z	16
$D_{\text{calcd}}/\text{g cm}^{-3}$	1.741
$\mu(\text{Mo-K}\alpha)/\text{cm}^{-1}$	25.2
$F(000)/e$	3760
hkl range	$-33 \leq h \leq 33; -19 \leq k \leq 20; -31 \leq l \leq 33$
Refl. observed/unique/ R_{int}	77 635/22 006/0.0623
Parm. refined	1145
$R(F)/wR(F^2)^a$ (all refls.)	0.0529, 0.1167
$\Delta\rho$ (max/min)/ $e \text{ \AA}^{-3}$	1.40/−1.56

$${}^a R_1 = \sum[|F_o| - |F_c|]/\sum|F_o|, wR_2 = [\sum w(|F_o|^2 - |F_c|^2)^2/\sum w(|F_o|^2)^2]^{1/2}.$$

Table 2 Photoluminescence data of as-synthesised and activated **1**

	as-Synthesised MOF	Activated MOF
Max. emission ($\lambda_{\text{Exc}} = 366 \text{ nm}$)	422 nm	425 nm
Max. excitation ($\lambda_{\text{Em}} = 422/425 \text{ nm}$)	367 nm	380 nm
CIE coordinates ³²		
x	0.150	0.149
y	0.059	0.066
Absolute QY ($\lambda_{\text{Exc}} = 366 \text{ nm}$)	55%	36%

activated MOF exhibit an additional minor emission maximum at $\lambda = 460 \text{ nm}$. We attribute this secondary band to multiple effects: Ce^{3+} shows splitting of the ground states (${}^2\text{F}_{5/2}$ and ${}^2\text{F}_{7/2}$ expected value = 2300 cm^{-1} according to ref. 27). As the observed value 1690 cm^{-1} is at the border of the reported energy gap even if a large literature deviation of $\pm 600 \text{ cm}^{-1}$ is considered, we also looked for additional non-metal based effects. In addition to the Ce^{3+} -ground state splitting, an emission of the deprotonated ligand imidazolate Im^- immobilised in the rigid framework may be another origin of the emission shoulder. Additional energy pathways, which are not observed for the free ligand, have been previously reported for ligands immobilised in the MOF structures.^{30,31} As 1*H*-imidazole does not show the related band, sodium imidazolate was prepared as a spectroscopic reference for the imidazolate anion (see Fig. S2, ESI†). Sodium imidazolate (NaIm) also shows the corresponding emission band without the ground-state splitting of Ce^{3+} . Accordingly, comparison between the emission maxima of ${}^3[\text{Ce}(\text{Im})_3\text{ImH}] \cdot \text{ImH}$ (**1**) and NaIm confirms that the minor maximum originates from the emission of anionic imidazolate in addition to the ground state splitting of Ce^{3+} .

The photoluminescence of **1** can be influenced by liquids like classic solvents and gases, thus providing potential for detection of the interacting species as analyte. Altogether,

eight different solvents were investigated by addition of the solvent to the MOF: water, methanol, acetone, pyridine, acetonitrile, dichloromethane, toluene and hexane under inert conditions in argon. Time dependent excitation and emission spectra were recorded subsequent to the addition of the respective solvent. They were then compared to the state of the pure MOF and the influence of the solvent on the luminescence was monitored.

In addition, the behaviour of the MOF in the presence of four different gases, namely Ar, N₂, CO₂ and O₂, was investigated. A sample cell filled with the compound that was previously activated *in vacuo* was flooded with the gas. Again, time dependent excitation and emission spectra were compared to the spectra of **1** to monitor the potential influence of the analyte gas.

The time-dependent luminescence investigations for solvents can be beneficially carried out with the purified as-synthesised MOF, sparing the full activation process. During our studies, it became evident that the time-dependence can be positively influenced by a molecule exchange process. Exchange processes elongate the time scale for solvents that cannot easily replace imidazole from the as-synthesised MOF. Therefore, a time-dependent selectivity is available. Moreover, sparing the full activation of the MOF simplifies potential application as a detector/sensor.

The investigation of the solvents shows a variable influence on the MOF photoluminescence depending on the character of the solvent: protic, polar, aprotic and non-polar. This results in intensity changes either being “turn-on” or “turn-off” effects. Up to now, contact times in hours, rather than time scale of detection have been reported in studies on luminescence sensing with MOFs. For this reason, we carried out time-dependent investigations on sensing with **1**. In order to avoid a concentration effect, the time-dependent investigations were carried out by direct contact with the analyte.

The luminescence is immediately and fully quenched upon addition of water in less than 3 s. The quenching, reaching λ_{\max} at 400 nm half-width <3 s, is faster than recording an emission spectrum, as proven by spectrometer parameters: range 380–650 nm, scan time 0.1 s nm⁻¹, 1 s integration time for the overall spectrum, giving an overall recording time of 28 s. Longer interaction with water does not further change the photoluminescence behaviour (see Fig. 6). This “turn-off” effect arises from the hydrolysis of the MOF and thus allows an irreversible detection of water. In contrast to other water-sensitive MOFs, the high speed of the process combined with the observable parameter of luminescence intensity loss renders **1** a suitable detector for water.

Irreversible detection of water can, *e.g.* be especially useful for detection systems that do not allow a reversible change of the detection signal, but instead rely on maintaining the detection grade for longer times. Such examples include water-sensitive pharmaceutical formulations, for which we are currently developing such sensors. For such pharmaceuticals reversible processes would enable possible unwanted re-drying and therefore a wrong detection signal. A wrong outcome of detec-

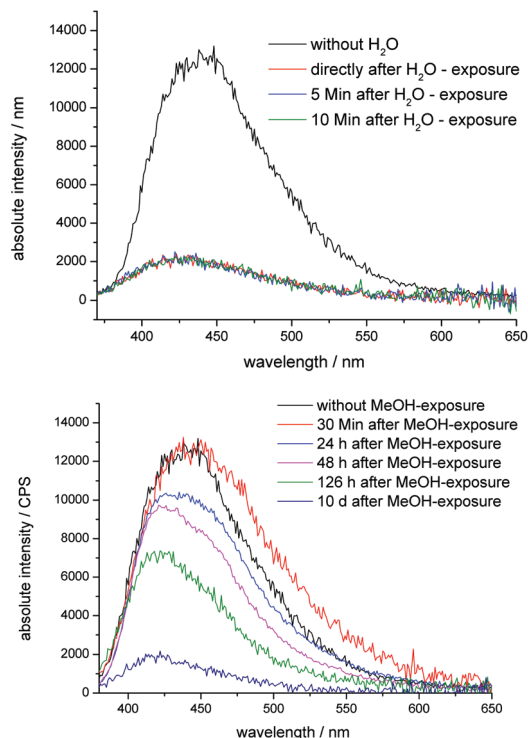


Fig. 6 Emission spectra of **1** as time dependent monitoring of the influence of H₂O (top) and MeOH on the emission intensity.

tion could easily happen as such products are not continuously monitored during storage. Accordingly, this kind of detection has to be irreversible.

In comparison with water, the protic solvent MeOH also gives a reduction of the emission intensity, but on a longer time scale. It takes 10 days to reduce the luminescence intensity by the same amount as water does instantaneously. Thus, water and MeOH as an alcohol can be clearly distinguished by a ratio of complete “turn-off” luminescence effect of >250 000 : 1. For methanol, 65% of the intensity is still present after 48 h and 15% after 10 days (see Fig. 6 and S3, ESI†).

The aprotic polar solvents acetone and pyridine (py) also show this gradual loss of the excitation and emission intensities; acetone taking one hour and pyridine six hours for an almost complete “turn-off” effect (see Fig. S4, S5, ESI†). This gives a time scale ratio of 1000 : 1 (acetone) and 6000 : 1 (py) when compared to water detection. For this reason, the time-dependence of an intensity-change can be used to increase the selectivity of the “turn-off” detection process.

Aside from the time-scale, another method used to distinguish the different “turn-off”-effects and thereby the analytes was the chromaticity of the emission according to CIE.³² These were determined as colour points after addition of each solvent. The colour point was determined when a stable value was reached and remains almost unchanged with the exception of the addition of methanol. Methanol addition shows a clear shift (see Fig. 7) compared to **1** or **1** with MeCN or pyridine (equal to a bathochromic shift of >20 nm). MeOH can

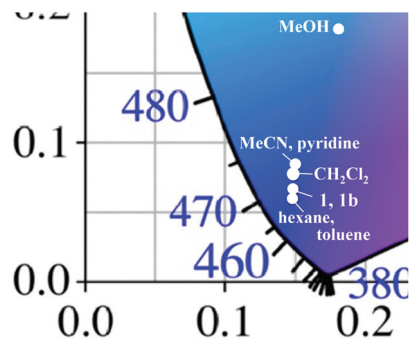


Fig. 7 Excerpt of the chromaticity diagram according to CIE showing the colour points of **1** after the addition of solvents.

therefore also be distinguished *e.g.* from MeCN and py; the time-dependence measurements do not allow for differentiation between these three solvents. Such irreversible “turn-off” effects can arise from dissolution of the MOF by coordination of the analyte, as *e.g.* pyridine complexes of the lanthanide are known.³³ The formation of Ln–pyridine coordination could occur due to acid–base adduct formation between the Lewis-base pyridine and the Lewis-acid Ce³⁺. An analogous process can of course also occur for protic solvents like MeOH and water, for which the fast irreversible hydrolysis are also observed. To identify potential products and residues of the MOF framework suspended in each solvent, powder diffraction experiments were carried out after evaporation of respective solvents, but gave only X-ray amorphous patterns. Therefore, the time-dependent loss in intensities of excitation and emission after addition of the respective solvent is a hint of an irreversible reaction of the analytes with the MOF compound **1**.

For the two aprotic, polar solvents acetonitrile and dichloromethane, interestingly a reversible “turn-on”-effect is detected for the excitation and emission intensities of **1** (see Fig. 8). This “turn-on”-effect for dichloromethane can be identified 10 minutes after solvent addition and yields an increase of 30% in overall intensity, reached after 1 h. For acetonitrile, a moderate intensity increase of 15%, reached after 2 h, was recorded after the addition of the solvent (see Fig. S6, ESI†). Both solvents can obviously act as additional sensitizers for the photoluminescence of the MOF feeding the Ce³⁺ emission by an energy transfer. These additional antenna effects are reasonable, as *e.g.* nitriles have already been shown to act as sensitizers for MOF-luminescence in the dinitriles ${}^3\infty[\text{LnCl}_3(1,3\text{-Ph}(\text{CN})_2)]$, Ln = Eu, Tb.³⁴ However, the amount of intensity increase is quite surprising for CH₂Cl₂ (see Fig. 8, S6, ESI,† for MeCN).

The time-scale observed for the reversible “turn-on” processes can also be attributed to the soaking process in which the analyte enters the MOF pores. This is a result of the interaction of the analyte molecules and the MOF influencing both time-dependence and absolute intensity change. Furthermore, photoluminescence spectra were also recorded for **1** in the aprotic, non-polar solvents toluene and hexane. The spectra

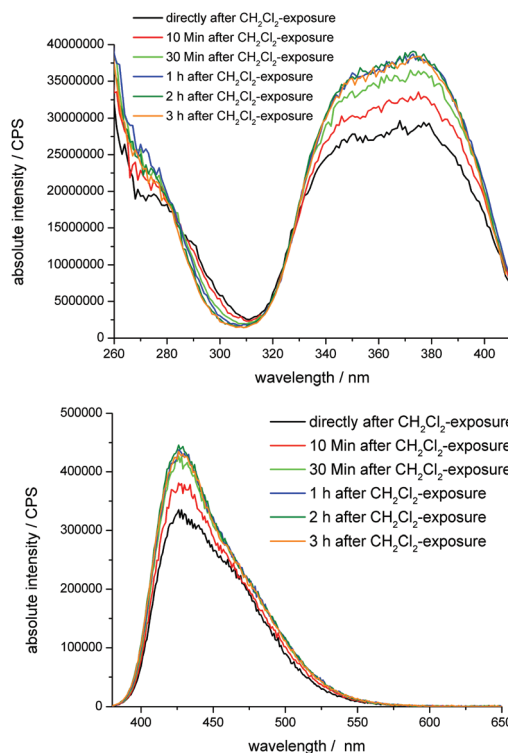


Fig. 8 Time dependent excitation (top) and emission (bottom) spectra of **1** in dichloromethane (CH₂Cl₂) indicating “turn-on”-effect of 30%.

show no change if it is dry and kept under inert conditions. As expected, this extends also to chromaticity (see Fig. 7).

Time dependent gas-sensing investigations of **1** were also carried out for the typical gas components of air: N₂, O₂, Ar, and CO₂. Therefore, a sample cell filled with compound **1**, previously activated *in vacuo*, was flooded with the analyte gas. An initial photoluminescence spectrum was recorded under vacuum conditions (10⁻⁵ mbar) prior to flooding of the sample cell up to a pressure of 99 992 Pa (750 mmHg) of the gas. Luminescence spectra were recorded every 300 s for one hour and compared to the spectra prior to gas application. The results are again dependent on the analyte indicating potential “turn-off” sensing for O₂ and to a lesser extent for CO₂ represented by a decrease in the luminescence intensity. No change or shift was observed in signal shape or position of the intensity maximum, respectively. Subsequently, all spectra were integrated over the full width of the observed range to obtain the absolute intensity decrease (380 nm to 650 nm, see Fig. 9). The integrated intensities were normalised to the reference spectrum recorded for the evacuated sample cell.

Intensity fluctuations with a magnitude of up to 4% were observed for both Ar and N₂ exposures at room temperature but these intensity changes are not thought to be significant. The deviations may be explained by a variety of minor error sources such as deviations occurring between flooding the sample cell with analyte gas from vacuum to 99 991.8 Pa (750 mmHg), mobility of the finely ground powder particles or fluctuations of the excitation beam intensity. It can be con-

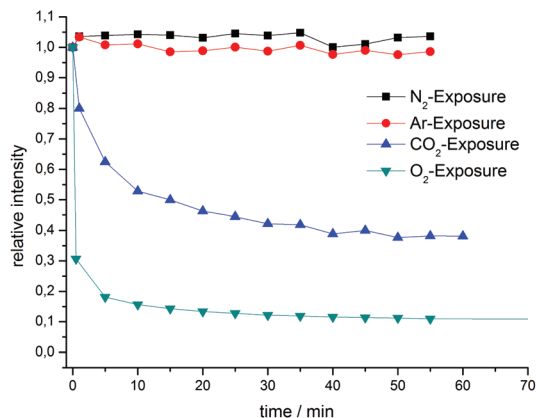


Fig. 9 Time-dependent integrated relative emission intensities of **1** for different gas exposures.

cluded that the MOF luminescence is not influenced by the gases Ar and N₂ within these deviations.

Exposure of the MOF to O₂ leads to a very sharp drop in intensity of 70% within seconds, and about 85% in 5 min. This behaviour follows an asymptotic function and may indicate a direct interaction of the oxophilic luminescent centres with O₂ and quenching of the luminescence processes by oxygen-presence within the coordination sphere of the Ce³⁺ centres. A weaker “turn-off”-behaviour can be observed for the exposure of **1** to CO₂ (99 992 Pa, 750 mmHg; see also Fig. 9), but reaches an intensity reduction to only 45% of the original intensity within an hour, and almost no change within the first minute. Both gases therefore show a “turn-off” effect that is clearly distinguishable by their time-/intensity-dependence, with O₂ being much more pronounced and spontaneous.

To identify potential chemical processes that might be responsible for the decrease of the emission intensities, subsequent to flooding and evacuating of the sample cell, powder diffraction investigations were carried out. In both powder diffractograms, the main reflections of the MOF (**1**) are present, giving evidence that the MOF structure is maintained (see Fig. S7, ESI[†]). Monitoring the CO₂-pressure within the sample cell during the exposure phase shows a loss of 1639.9 Pa (12.3 mmHg) within the first 60 minutes of the experiment and a loss of 5732.9 Pa (43.0 mmHg) after an exposure of 24 hours. This is consistent with the equilibration times observed in the BET experiment, which may be the explanation for the much slower detection/luminescence change of/by CO₂. In order to check for a reversible sensing, the sample cell was evacuated for an extended period of time (*e.g.* 72 h) and a final spectrum was recorded. However, the intensity observed remained at the reduced intensity values resulting from the exposure to CO₂ and O₂. As the crystal structure does not change no chemical reaction is taking place, different from exposure to water. This indicates the occurrence of a chemical sorption that cannot be reversed by simple evacuation. As the lanthanides are highly oxophilic this observation also hints that when the gases enter the proximity of the Ce³⁺-ions, they act as quenchers. This quenching is not possible by N₂ and Ar.

With regard to the ratio of O₂ and CO₂ in air, **1** can be used as a detector for oxygen in dry air, as the low amount of CO₂ in air hardly influences the result giving a deviation/error of <1% of the detection signal.

Conclusions

A novel blue luminescent MOF ³[Ce(Im)₃(ImH)]-ImH was achieved *via* solvent-free redox reaction of the linker 1*H*-imidazole and elemental cerium. The as-synthesised MOF can be activated to give the microporous constitution ³[Ce(Im)₃-(ImH)]. The intense blue luminescence results from parity allowed 5d–4f-transitions and is retained upon activation. Absolute quantum yields were determined for the as-synthesised and the activated form of the MOF reaching 55% for the non-activated due to a sensitization effect of imidazole in the pores. Removal of these molecules reduces the quantum yield to 36%. The luminescent MOF can be utilised as a potential sensor/detector for O₂ in dry air and H₂O by a significant “turn-off”-effect of the luminescence. Another application lies in the detection of CO₂ in the absence of the other two analytes. In general, “turn-off”-effects can be observed for protic and polar solvents. Time-dependent investigations show a high-speed detection (<3 s) for water only, whereas MeOH, acetone, pyridine show a much longer period for the time-dependent “turn-off”. Selectivity can thereby be achieved by the high ratio of the time-dependent signal change, which ranges up to 250 000 : 1 for H₂O–MeOH.

The purified as-synthesised MOF can be directly used as a detector with good time-dependent selectivity, as the exchange process of intercalated molecules in the pore system enhances the time scale. The complex activation process can be omitted, whereas gas detection depends on the accessibility of the pore system. The “turn-off”-effects of the analytes MeOH, py and acetone can be further distinguished by a shift in the chromaticity, especially for MeOH. The chromaticity of the luminescence shifts to higher wavelengths with increasing polarity of the analyte. In contrast to “turn-off”, the analyte molecules acetonitrile and dichloromethane provoke a “turn-on”-effect of the luminescence by acting as sensitizers. For the gases constituting dry air, PXRD shows that the MOF structure is maintained, whereas the speed of the water detection is attributed to an extremely rapid hydrolysis. This is useful for all processes in which an irreversible signal change is desired (*viz.* that should not be changed upon re-drying).

Due to the spontaneous character and impact strength of the “turn-off”-effect, the novel cerium-MOF can be used as a rapid luminescence detector for water and oxygen. This is especially the case for water detection as the as-synthesised MOF can be directly utilised. To the best of our knowledge, this is the first example utilising 5d–4f-transitions for detection with MOFs. Altogether, this report distinguishes and compares irreversible detection from reversible sensing for the different “turn-off” and “turn-on” effects reported including chemical reactions like hydrolysis, chemisorption and revers-

ible interaction, as all of them can be useful depending on the sensing/detection requirements.

Experimental

Synthesis of ${}^3[\text{Ce}(\text{Im})_3\text{ImH}]\cdot\text{ImH}$ (**1**)

The compound ${}^3[\text{Ce}(\text{Im})_3\text{ImH}]\cdot\text{ImH}$ (**1**) was synthesized *via* a solvent-free reaction in a self-consuming organic melt of 1*H*-imidazole. All reagents were used as purchased. Freshly filed Ce-metal (99.9%, Smart elements, 1 mmol, 140 mg) and 1*H*-imidazole (99.5%, Sigma Aldrich, 5 mmol $\text{C}_3\text{N}_2\text{H}_4$, 340 mg) were sealed in an evacuated DURAN® glass ampoule (1×10^{-3} mbar). The reaction mixture was heated in a resistance tube oven from room temperature to 190 °C within 3 hours. The temperature was kept constant for 72 h and then cooled to room temperature within 12 h. To achieve complete reaction, the mixture was ground with further 1*H*-imidazole (1 mmol, 68 mg), sealed and heated again, using the heating program described above. Excess 1*H*-imidazole was removed *via* sublimation. The remaining product was a colourless fine powder of **1**. Yield: 353 mg = 74% Anal. calcd for $\text{C}_{15}\text{H}_{17}\text{N}_{10}\text{Ce}$ ($M_r = 477.51 \text{ g mol}^{-1}$): C, 37.73; N, 29.33; H, 3.59. Found C, 36.62; N, 28.24; H, 3.42%. MIR (KBr): (3358 m, 3124 m, 3021 m, 2918 m, 2827 m, 1677 w, 1596 w, 1528 w, 1456 s, 1419 m, 1321 w, 1304 w, 1252 m, 1231 m, 1141 m, 1078 bs, 954 w, 933 s, 836 m, 754 m, 675 s, 661 m, 621 w, 595 m) cm^{-1} . FIR (PE): (192 w, 157 w, 142 w, 130 w, 116 vs) cm^{-1} .

X-Ray diffraction

A suitable crystal of ${}^3[\text{Ce}(\text{Im})_3\text{ImH}]\cdot\text{ImH}$ was selected for the single crystal X-ray analysis in a glovebox and sealed in a glass capillary. The data collection was carried out on a STOE IPDS-I diffractometer ($\text{MoK}\alpha$ radiation $\lambda = 0.7107 \text{ \AA}$) at 140(1) K. The structure was determined using direct methods.³⁵ The non-H atoms were refined anisotropically by least squares techniques.³⁶ The positions of the hydrogen atoms were refined isotropically for all framework H-atoms and derived from pre-calculated positions using a riding model for the intercalated imidazole molecule. The compound crystallizes in the monoclinic crystal system in the centro symmetric space group $P2_1/n$. Integrity of the symmetry and geometry were checked.³⁷ Crystallographic data for the crystal X-ray determination are summarized in Table 1.

Powder samples were prepared in Lindemann glass capillaries ($\text{Ø} = 0.3 \text{ mm}$) under an inert gas atmosphere. The powder diffractograms were recorded on a Bruker D8 Discover with *Da Vinci* design and LynxEye detector in transmission geometry with a focusing Göbel mirror with $\text{CuK}\alpha$ -radiation ($\lambda = 1.54056 \text{ \AA}$). For investigation of the residues of the liquid sensing photoluminescence spectroscopy, the respective solvent was evaporated under vacuum and the powder diffractograms were recorded on a Si-waver in reflection geometry with $\text{CuK}\alpha$ -radiation ($\lambda = 1.54056 \text{ \AA}$).

Photoluminescence spectroscopy & quantum yield determination

Excitation and emission spectra were recorded with a Horiba Jobin Yvon Fluorolog 3 photoluminescence spectrometer with 450 W Xe lamp, an integration sphere, Czerny–Turner double grating (1200 grooves per mm) excitation and emission monochromators and an FL-1073 PMT detector.

Excitation spectra were recorded from 250 to 410 nm and corrected for the spectral distribution of the lamp intensity using a photodiode reference detector. Emission spectra were recorded from 380 to 650 nm and corrected for the spherical response of the monochromators and the detector using typical correction spectra provided by the manufacturer.

The quantum yield was also recorded using a photoluminescence spectrometer Horiba Jobin Yvon Spex Fluorolog 3, equipped with a 450 W xenon lamp, double monochromators for excitation and emission, an integrating sphere (Ulbricht sphere) and a photomultiplier as the detector. For excitation wavelengths $>330 \text{ nm}$, the absolute quantum yield was determined according to Friend.³⁸ First the diffuse reflection of the sample was determined at a certain excitation wavelength. Second, the emission was measured under excitation at the same wavelength. Integration of the reflected and emitted photons by use of the Ulbricht sphere resulted in the absolute quantum yield. Corrections were made accounting for the spectral power of the excitation source, the reflection behaviour of the Ulbricht sphere, and the sensitivity of the detector. For excitation wavelengths $<330 \text{ nm}$, the reflectivity of the Ulbricht sphere starts to be perceptibly below 100%, resulting in a less precise determination of the absolute quantum yield. Therefore, the relative quantum yield was determined by comparison with a fluorescent lamp phosphor with a defined quantum yield. Here, $\text{BaMgAl}_{10}\text{O}_{17}:\text{Eu}^{2+}$ (BAM:Eu²⁺) (Philips) was used as a reference.³⁹

Sensing/detection investigations

For the potential luminescence sensing of solvents, ${}^3[\text{Ce}(\text{Im})_3\text{ImH}]\cdot\text{ImH}$ (**1**) and a mini agitator were placed under inert conditions in a quartz cuvette, which was sealed with a septum and additional wrapping with Parafilm®. Directly after the addition of the relative solvent excitation and emission spectra were recorded. The used solvents were dried under standard conditions (except water and acetone). The sample cell was coupled with a Horiba Fluorolog-3 photoluminescence spectrometer *via* a fibre-optic cable. This assembly allows photoluminescence experiments with solid/liquid mixtures under reflection conditions, while the Ce-imidazolite was stirred in order to provide contact between liquid phase and the framework particles.

The used eight solvents were purified and dried under standard conditions (except water which was used as distilled water and acetone which was used as purchased): dried methanol: pre-dried using magnesium chips and iodine followed by distillation; pyridine: left over molecular sieves 4 \AA for several days; acetonitrile: distillation over P_2O_5 ; dichloromethane: left

over CaCl_2 overnight and then distilled over P_2O_5 ; toluene: distillation over CaH_2 ; hexane: left over 24 hours over CaCl_2 and then distilled over P_2O_5 .

For potential gas detection, **1** was placed under inert conditions in a specially designed L-shaped sorption cell of a Quantachrome Autosorb AS-1c. The glass ceiling of the sample cell was made from Suprasil glass, which is suitably transparent for photoluminescence experiments including the UV-VIS region. The sample cell was then coupled with a Horiba Fluorolog-3 photoluminescence spectrometer via a fibre-optic cable, allowing photoluminescence experiments under reflection conditions, while the sample cell was flooded with gas handled by a Quantachrome Autosorb AS-1c. Experiments were carried out for Ar (Fa. Linde Gas, purity 5.0), N_2 (Fa. Linde Gas, purity 5.0) and CO_2 (Fa. Linde gas, purity 5.0). The spectra were obtained at an excitation wavelength of 363 nm and emission was measured between 380 nm and 650 nm with incremental steps of 1 nm.

Thermal and elemental analysis

For thermal analysis the bulk material of the synthesis of $^3[\text{Ce}(\text{Im})_3\text{ImH}]\text{-ImH}$ was purified by evaporation of excess 1*H*-imidazole at 110 °C under vacuum. The thermal properties were investigated by simultaneous DTA/TG (Netzsch STA 409, Proteus Software), using 34 mg of sample. The sample was kept under an inert gas atmosphere (50% Ar and 50% N_2) and heated from 25 to 950 °C at a heating rate of 10 °C min^{-1} . Elemental analysis for C, H and N was performed with a Euro Ea CHNSO Analyzer (HEKATECH GmbH).

Gas adsorption properties

Volumetric uptake and specific surface areas were determined by adsorption–desorption isotherms of different gases (−196 °C for N_2 , 99.999% and Ar, 99.999%, as well as −75° C for CO_2 , 99.9993% and −153° C for Kr, 99.996%) obtained on a Quantachrome Autosorb 1C apparatus according to the BET theory. Prior to the adsorption measurements, the samples were degassed at a vacuum of 10^{-3} mbar for 4.5 h at 225 °C. The results were compared to the non-activated framework **1**.

Vibrational spectroscopy

FTIR spectra in the MIR area were recorded using a Thermo Nicolet FTIR-380 spectrometer; samples were measured in dried KBr pellets under inert conditions. Spectra in the FIR area were recorded using a Bruker FTIR-IS66V-S spectrometer and the samples were measured in dried PE-pellets.

Acknowledgements

Support by the *Deutsche Forschungsgemeinschaft* within the priority program SPP1362 “Metal–Organic Frameworks” is gratefully acknowledged.

Notes and references

- (a) B. F. Hoskins and R. Robson, *J. Am. Chem. Soc.*, 1989, **111**, 5962; (b) B. F. Hoskins and R. Robson, *J. Am. Chem. Soc.*, 1990, **112**, 1546.
- (a) G. Ferey, *Chem. Soc. Rev.*, 2008, **37**, 191; (b) J. R. Long and O. M. Yaghi, *Chem. Soc. Rev.*, 2009, **38**, 1213; (c) L. J. Murray, M. Dincă and J. R. Long, *Chem. Soc. Rev.*, 2009, **38**, 1294; (d) C. Janiak and J. K. Vieth, *New J. Chem.*, 2010, **34**, 2366.
- (a) O. M. Yaghi, H. Li, C. Davis, T. Richardson and T. L. Groy, *Acc. Chem. Res.*, 1998, **31**, 474; (b) S. Kitagawa and M. Kondo, *Bull. Chem. Soc. Jpn.*, 1998, **71**, 1739; (c) H. Le, M. Eddaoudi, M. O’Keefe and O. M. Yaghi, *Nature*, 1999, **402**, 276; (d) G. Ferey, *Chem. Mater.*, 2001, **13**, 3084; (e) C. Janiak, *Dalton Trans.*, 2003, 2781; (f) S. Kitagawa and K. Uemura, *Chem. Soc. Rev.*, 2005, **34**, 109; (g) S. Kaskel, *Nachr. Chem.*, 2005, **53**, 394; (h) A. K. Cheetham and C. N. R. Rao, *Science*, 2007, **318**, 58.
- S. Kitagawa, R. Kitaura and S. Noro, *Angew. Chem., Int. Ed.*, 2004, **43**, 2334.
- M. Kurmoo, *Chem. Soc. Rev.*, 2009, **38**, 1353.
- M. Yoon, R. Srirambalaji and K. Kim, *Chem. Rev.*, 2012, **112**, 1196.
- (a) D. F. Sava, L. E. S. Rohwer, M. A. Rodriguez and T. M. Nenoff, *J. Am. Chem. Soc.*, 2012, **134**, 3983; (b) A. Ablet, S.-M. Li, W. Cao, X.-J. Zheng, W.-T. Wong and L.-P. Jin, *Chem. – Asian J.*, 2013, **8**, 95; (c) P. Falcaro and S. Furukawa, *Angew. Chem., Int. Ed.*, 2012, **51**, 8431; (d) M. D. Allendorf, C. A. Bauer, R. K. Bhakta and R. J. T. Houk, *Chem. Soc. Rev.*, 2009, **38**, 1330.
- P. R. Matthes, C. J. Höller, M. Mai, J. Heck, S. J. Sedlmaier, S. Schmiechen, C. Feldmann, W. Schnick and K. Müller-Buschbaum, *J. Mater. Chem.*, 2012, **22**, 10179.
- J.-C. Rybak, L. V. Meyer, J. Wagenhöfer, G. Sextl and K. Müller-Buschbaum, *Inorg. Chem.*, 2012, **51**, 13204.
- (a) L. E. Kreno, K. Leong, O. K. Farha, M. Allendorf, R. P. Van Duyne and J. T. Hupp, *Chem. Rev.*, 2012, **112**, 1105; (b) J. Lei, R. Qian, P. Ling, L. Cui and H. Ju, *Trends Anal. Chem.*, 2014, **58**, 71.
- (a) D. Liu, K. Lu, C. Poon and W. Lin, *Inorg. Chem.*, 2014, **53**, 1916; (b) Z. Hu, B. J. Deibert and J. Li, *Chem. Soc. Rev.*, 2014, **43**, 5815.
- Z. Xie, L. Ma, K. E. deKrafft, A. Jin and W. Lin, *J. Am. Chem. Soc.*, 2009, **132**, 922.
- (a) A. Lan, K. Li, H. Wu, D. H. Olson, T. J. Emge, W. Ki, M. Hong and J. Li, *Angew. Chem., Int. Ed.*, 2009, **48**, 2334; (b) S. Pramanik, C. Zheng, X. Zhang, T. J. Emge and J. Li, *J. Am. Chem. Soc.*, 2011, **133**, 4153.
- X. Zhou, H. Li, H. Xiao, L. Li, Q. Zhao, T. Yang, J. Zuo and W. Huang, *Dalton Trans.*, 2013, **42**, 5718.
- Z. Liu, W. He and Z. Guo, *Chem. Soc. Rev.*, 2013, **42**, 1568.
- Y. Takashima, V. M. Martinez, S. Furukawa, M. Kondo, S. Shimomura, H. Uehara, M. Nakahama, K. Sugimoto and S. Kitagawa, *Nat. Commun.*, 2011, **2**, 168.

- 17 (a) B. Chen, L. Wang, Y. Xiao, F. R. Fronczek, M. Xue, Y. Cui and G. Qian, *Angew. Chem., Int. Ed.*, 2009, **48**, 500; (b) Y.-Y. Jiang, S.-K. Ren, J.-P. Ma, Q.-K. Liu and Y.-B. Dong, *Chem. – Eur. J.*, 2009, **15**, 10742.
- 18 K. Müller-Buschbaum, *Z. Anorg. Allg. Chem.*, 2005, **631**, 811.
- 19 K. Müller-Buschbaum, S. G. Torres, P. Larsen and C. Wickleder, *Chem. Mater.*, 2007, **19**, 655.
- 20 A. Zurawski, M. Mai, D. Baumann, C. Feldmann and K. Müller-Buschbaum, *Chem. Commun.*, 2011, **47**, 496.
- 21 A. Zurawski, J.-C. Rybak, L. V. Meyer, P. R. Matthes, V. Stepanenko, N. Dannenbauer, F. Würthner and K. Müller-Buschbaum, *Dalton Trans.*, 2012, **41**, 4067.
- 22 J.-C. Rybak, M. Hailmann, P. R. Matthes, A. Zurawski, J. Nitsch, A. Steffen, J. G. Heck, C. Feldmann, S. Götzendörfer, J. Meinhardt, G. SEXTL, H. Kohlmann, S. J. Sedlmaier, W. Schnick and K. Müller-Buschbaum, *J. Am. Chem. Soc.*, 2013, **135**, 6896.
- 23 K. Müller-Buschbaum, *Z. Naturforsch.*, 2006, **61b**, 792.
- 24 K. Müller-Buschbaum and Y. Mokaddem, *Eur. J. Inorg. Chem.*, 2006, 2000.
- 25 X.-L. Zheng, Y. Liu, M. Pan, X.-Q. Lü, J.-Y. Zhang, C.-Y. Zhao, Y.-X. Tong and C.-Y. Su, *Angew. Chem., Int. Ed.*, 2007, **46**, 7399.
- 26 R. S. Rowland and R. Taylor, *J. Phys. Chem.*, 1996, **100**, 7384.
- 27 P. Dorenbos, *J. Lumin.*, 2000, **91**, 91.
- 28 S. P. Nakamura, *Soc. Photo-Opt. Ins.*, 1997, **3002**, 26.
- 29 E. Bernarducci, P. K. Bharadwaj, K. Krogh-Jespersen, J. A. Potenza and H. J. Schugar, *J. Am. Chem. Soc.*, 1983, **105**, 3860.
- 30 Y. Cui, Y. Yue, G. Qian and B. Chen, *Chem. Rev.*, 2012, **112**, 1126.
- 31 Y. Cui, B. Chen and G. Qian, *Coord. Chem. Rev.*, 2014, **273–274**, 76.
- 32 A. Broadbent, *Color Res. Appl.*, 2004, **29**, 267.
- 33 (a) W. J. Evans, D. G. Giarikos and J. W. Ziller, *Organometallics*, 2001, **20**, 5751; (b) J.-S. Li, B. Neumüller and K. Dehnicke, *Z. Anorg. Allg. Chem.*, 2002, **628**, 45; (c) G. B. Deacon, N. M. Scott, B. W. Skelton and A. H. White, *Z. Anorg. Allg. Chem.*, 2006, **632**, 1945; (d) J.-S. Li, B. Neumüller and K. Dehnicke, *Z. Anorg. Allg. Chem.*, 2002, **628**, 2785.
- 34 C. J. Höller, P. R. Matthes, M. Adlung, C. Wickleder and K. Müller-Buschbaum, *Eur. J. Inorg. Chem.*, 2012, 5479.
- 35 G. M. Sheldrick, *SHELXS-97, Program for the solution of crystal structures*, Göttingen, 1997.
- 36 G. M. Sheldrick, *SHELXL-97, Program for the refinement of crystal structures*, Göttingen, 1997.
- 37 (a) A. L. Spek, *PLATON-2000, A Multipurpose Crystallographic Tool*, Utrecht, 2000; (b) *XPREP v6.12, Program for symmetry analysis and data reduction of diffraction experiments*, Bruker AXS Inc., Madison, USA, 2001.
- 38 J. V. de Mello, H. F. Wittmann and R. H. Friend, *Adv. Mater.*, 1997, **9**, 230.
- 39 (a) A. L. I. Stevels and A. J. M. Schrama de Pauw, *J. Electrochem. Soc.*, 1974, **123**, 691; (b) S. Marks, J. Heck, P. O. Burgos, C. Feldmann and P. W. Roesky, *J. Am. Chem. Soc.*, 2012, **134**, 16983.